Self-Healing Coating with a Controllable Release of Corrosion Inhibitors by Using Multifunctional Zinc Oxide Quantum Dots as Valves

Zhaowen Tian, Suning Li,* Yiqing Chen,* Lixiang Li, Zhizheng An, Yanqiu Zhang, Anqi Tong, Han Zhang, Zunfeng Liu,* and Baigang An*

Read Online

ACCESS | Metrics & More | Article Recommendations | Supporting Information

ABSTRACT: As an intelligent response system, self-healing anticorrosion materials containing nanocontainers have aroused increasing demands. It is highly expected that the nanocontainers can rapidly respond on corrosion signals to efficiently release corrosion inhibitors, meanwhile to avoid an undesirable leakage before the local corrosion happening. Herein, zinc oxide quantum dot (ZnO-QD)-sealed hollow mesoporous TiO_2 nanocontainers loading with 14.2% benzotriazole (BTA) inhibitor have been successfully prepared [hollow mesoporous titanium dioxide nanospheres (HMTNs)−BTA@ZnO-QDs]. ZnO-QDs play the multifunctional roles on anticorrosion of the self-healing coating. The corrosion tests of coatings on the carbon steel well demonstrate that ZnO-QDs can not only act as a valve to seal and release BTA on the time but also act as a precursor to produce the protective film of $Zn(OH)_2$ by the reaction of Zn^{2+} ions with OH^- around the cathode region to inhibit the corrosion of carbon steel. After being soaked in 3.5% NaCl solution for 30 days, the $|Z|_{0.01\ Hz}$ value of the coating with HMTNs−BTA@ZnO-QDs still maintains at $2.87 \times 10^7\ \Omega\ cm^2$. Once the defects are formed in the coating, the acid-responsive ZnO-QD valves are rapidly decomposed to release BTA inhibitor; meanwhile, the resulted $Zn(OH)_2$ layer prevent the carbon steel substrate from corrosion in the cathode area. Therefore, it could be promising that the present design of the nanocontainers matching with the multifunctional ZnO-QDs can offer a valuable strategy to construct the self-healing and anticorrosion coatings with a multiresponse to the corrosion environment.

KEYWORDS: nanocontainers, ZnO quantum dots, self-healing, corrosion, inhibitor
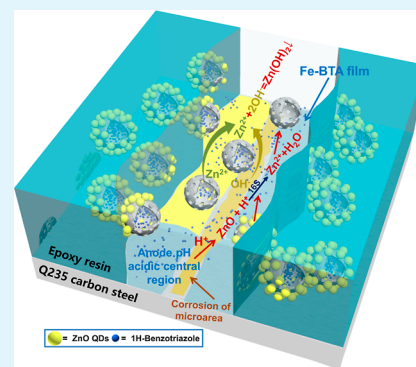
1. INTRODUCTION

Corrosion of metals causes inestimable losses throughout the world due to the spontaneity of chemical reactions.[1,2] Generally, organic coatings are used to avoid direct contact of metal substrates with electrolytes and air, which can prevent metals from corrosion.[3−5] However, once microcracks are produced on coatings, the corrosion will spread along the microcracks, leading to the failure of coatings.[6,7] Inspired by the self-healing properties of natural organisms that can respond to damage and then repair promptly, the self-healing coatings have attracted a great deal of interest.[8,9] During corrosion, the self-healing coatings involve two types of key materials: corrosion inhibitors and nanocontainers.[10−12] The latter are mainly used for storage of corrosion inhibitors, which can release the inhibitors to prevent the corrosion from proceeding by providing a shield once they sense the corrosion behavior of surroundings.[13,14]

As far as nanocontainers containing inhibitors are concerned, they are expected to own the following characteristics: (1) a large specific surface area and pore volume to fill and distribute the corrosion inhibitor, uniformly; (2) a stable physicochemical property to avoid the leakage of the corrosion inhibitor;[15,16] and (3) a prompt response to release the inhibitor. However, there are a couple of contradictions to avoid the unexpected leakage and to ensure the on-demand release of the corrosion inhibitor from the nanocontainers.[11,17] Porosity of nanocontainers can supply space to store the corrosion inhibitor, but the open pores also give inhibitors the channel to leak. Thereby, gatekeepers or switchers have been studied and used to seal and release inhibitors. Supramoleculars[12] and some organic functional groups grafted onto the surface of nanocontainers can provide a steric hindrance to block the leakages and to release inhibitors by the volume changes or a cyclic ring structure through a response on external stimuli including pH value, corrosion potential, UV
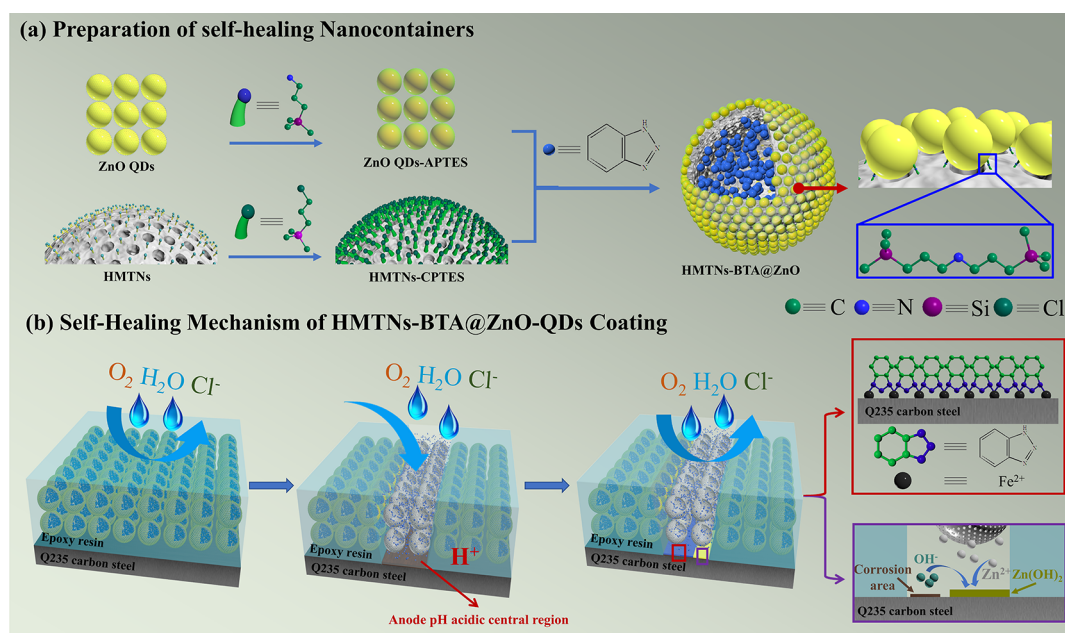
Figure 1. (a) Schematic preparation of ZnO-QDs−APTES and HMTNs−BTA@ZnO-QDs; (b) schematic representation of the self-healing mechanism of coating.

light, and redox.[18−23] However, it is quite difficult to match each molecule with the pore of porous nanocontainers. Some inorganic matters such as SiO_2 film[24] and ZnO nanoparticles were also applied as gatekeepers and to release inhibitors by the response on pH value of environments.[25,26] However, the response is limited by the dissolution rate of the inorganic materials, which could affect the prompt release of inhibitors. On the other hand, it would be more helpful on the anticorrosion property of the coating if the inorganic gatekeeper can also play corrosion inhibition roles. Quantum dot materials have shown advantages in some fields including drug transport and sensors. ZnO quantum dots (ZnO-QDs) had been successfully used as lids on anticancer drug-loaded mesoporous silica nanoparticles[27] since ZnO is stable in neutral solution and can be easily dissolved in an acid environment. Moreover, both ZnO and Zn^{2+} are biologically friendly, and some compounds including $Zn(OH)_2$, ZnO, and $ZnCO_3$ had been proved to have the protective property on inhibiting corrosion of metals.[28−30] ZnO-QDs have the superiority to match the pores of nanocontainers with several nanometers and meanwhile can be quickly decomposed in acid solutions. Therefore, it owns big potential to be used as a gatekeeper for nanocontainers. However, applications and effects of ZnO-QDs on self-sealing coatings are still rarely reported.

Herein, ZnO-QDs are used as the nanovalves to controllably release BTA inhibitors loaded in the hollow mesoporous titanium dioxide nanospheres (HMTNs), as illustrated in Figure 1, where ZnO-QDs with a size of 6.0 nm well match the pores of HMTNs to seal the BTA inhibitors into HMTNs and can sensitively respond the pH value of the environment to promptly release BTAs. Moreover, ZnO-QDs can act as a precursor to produce the protective layers containing Zn-$(OH)_2$ and ZnO, which makes the coating with HMTNs−BTA@ZnO-QDs have the anticorrosion property in both the basic and acid corrosion environments. Therefore, when HMTNs−BTA@ZnO-QDs are applied in the epoxy coating,

the coating exhibits an excellent self-healing property and anticorrosion performance.

2. EXPERIMENTAL SECTION

2.1. Materials. Ammonia (ammonium hydroxide), ethanol, methanol, ethyl orthosilicate (TEOS), and potassium hydroxide were purchased from Sinopharm Chemical Reagent Co., Ltd. Dimethyl sulfoxide was purchased from Liaoning Quanrui Reagent Co., Ltd. Toluene was provided by Beijing Chemical Plant Co., Ltd. Benzotriazole (BTA), tetrabutyl titanate (TBOT), and hydroxypropyl cellulose (HPC) were purchased from Shanghai Aladdin Reagent Co., Ltd. Polyvinylpyrrolidone (PVP, M_w ~40,000), 3-chloropropyltriethoxysilane (CPTES), zinc acetate dihydrate, and aminopropyl triethoxysilane (APTES) were purchased from Energy Chemical. Epoxy resin (E44) and the curing agent (704) were provided by Shanghai Macklin Biochemical Co., Ltd.

2.2. Preparation of ZnO-QD Valves Controlled Self-Healing Nanocontainers. *2.2.1. Preparation of Hollow Mesoporous Titanium Dioxide Nanospheres.* HMTNs were prepared by silica-protected calcination methods according to the literature with minor modification.[31] The experimental procedures are as follows:

Deionized water (10 mL) and ammonia solution (2 mL) were added to ethanol (75 mL) and vigorously stirred for 30 min. After TEOS (3 mL) was added, the mixture was stirred at room temperature for another 12 h. A solid SiO_2 powder was obtained by centrifugation and washed with ethanol and deionized water in sequence; then it was added to a mixed solution containing ethanol (20 mL), deionized water (100 μL), and hydroxypropyl cellulose (HPC, 120 mg), followed by stirring for 30 min, and then tetrabutyl titanate (TBOT, 2 mL) was slowly added and stirred under reflux at 85 °C for 2 h. The precipitate was isolated using centrifugation and washed with ethanol to obtain SiO_2@TiO_2 composites. In order to increase the thickness of the TiO_2 layer, the above coating procedure was repeated multiple times. Then it was dispersed in a mixture of water (20 mL) and polyvinyl pyrrolidone (PVP, M_w ~40,000, 400 mg) overnight so that PVP could be adsorbed on the surface of TiO_2. The precipitate was collected by centrifugation and dispersed in a mixed solution containing ethanol (15 mL), water (4.5 mL), and ammonia (0.28%, 650 μL) and stirred at room temperature for 30 min; finally, TEOS (860 μL) was added. The resulting SiO_2@TiO_2@SiO_2 particles were stirred for 8 h and centrifuged. After calcining at 800 °C for 2 h, SiO_2@TiO_2@SiO_2 products were chemically etched
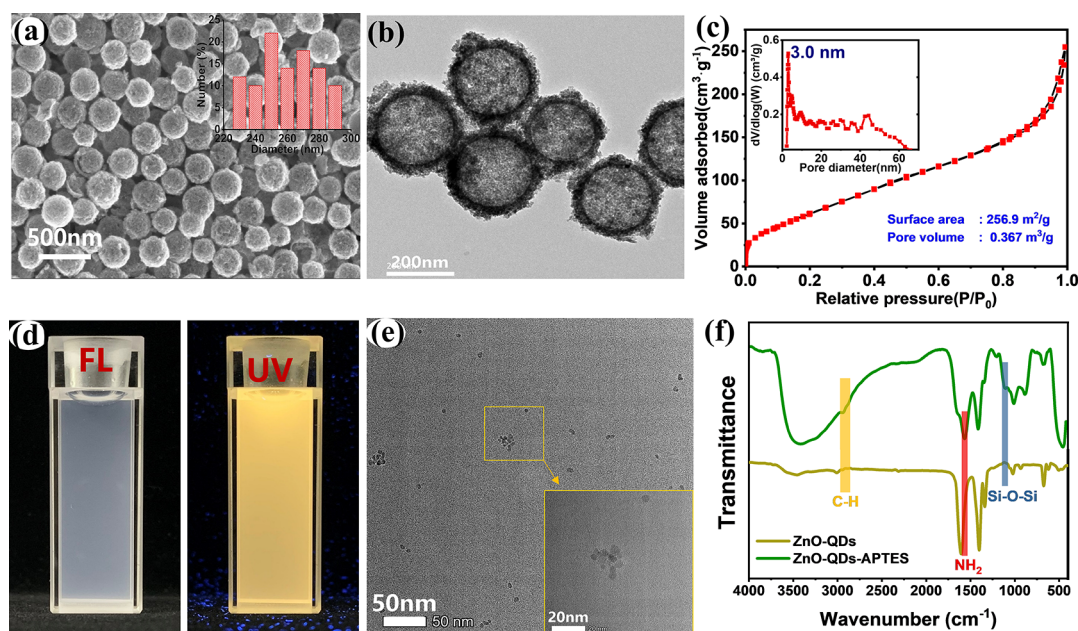
Figure 2. (a,b) SEM and TEM images of HMTNs synthesized by silica-protected calcination; (c) N_2 adsorption–desorption isotherm and pore size distribution curve of HMTNs; (d) state of ZnO-QDs in the presence of the UV lamp and daylight; (e) TEM images of ZnO-QDs; (f) FT-IR spectra of ZnO-QDs and ZnO-QDs–APTES.

by NaOH (5 mL, 5 mol/L) at 70 °C to remove silica-based materials. Finally, HMTNs were washed with abundant water and ethanol alternatively and dried under vacuum for further use.

2.2.2. Preparation of 3-Chloropropyltriethoxysilane-Modified Hollow Mesoporous Titanium Dioxide Nanospheres (HMTNs– CPTES). HMTNs (200 mg) were suspended in anhydrous toluene (20 mL). CPTES (100 μL) was added dropwise to the mixture, and the suspension was stirred under refluxing in a N_2 atmosphere overnight. The HMTNs–CPTES was separated by centrifugation, washed with anhydrous toluene and methanol, and dried under vacuum at 60 °C overnight.

2.2.3. Preparation of Amino-Functional ZnO-QDs (ZnO-QDs– APTES). Zinc acetate dihydrate (2.6 g) was added to anhydrous ethanol (75 mL) and stirred at 80 °C until zinc acetate was completely dissolved. When the temperature dropped to 50 °C, an ethanol solution of KOH (10 mL, 1.75 mol/L) was slowly added. The mixture of APTES (200 μL) and water (2 mL) was slowly added into the appellate ZnO-QD solution. Subsequently, a large amount of white precipitation was generated, which was collected by centrifugation, washed with a large amount of ethanol, and finally dispersed in anhydrous ethanol (10 mL) to obtain the milky white solution (Figure 1a).

2.2.4. Preparation of ZnO-QD Valve-Controlled Self-Healing Nanocontainers. 200 mg of HMTNs with 50 mL (10 mg/mL) of BTA saturated ethanol solution was stirred continuously under vacuum for 2 h and then cycled back to atmospheric pressure. This process was repeated thrice to improve the loading efficiency. By centrifugation, HMTNs–BTA was obtained.

The obtained HMTNs–BTA was dispersed in dimethyl sulfoxide (DMSO, 10 mL) and stirred for 30 min at room temperature. Then an ethanol solution of 2 mL ZnO-QDs was added, and the mixture was refluxed and stirred for 12 h at 60 °C in a N_2 atmosphere. HMTNs–BTA@ZnO-QDs was collected by centrifugation, washed with DMSO and methanol, and dried overnight at 60 °C under vacuum.

2.3. Preparation of Self-Healing Anticorrosion Coatings. Q235 (40 × 20 × 2 mm) carbon steel is used as the base material for anticorrosion coating. In order to clean and create a uniform layer on the surface of the substrate, the carbon steel plate was mechanically ground with 600, 800, 1000, and 1500 particle emery paper, ultrasonically cleaned in ethanol, and finally blow-dried with nitrogen

before experiments. The HMTNs–BTA@ZnO-QDs (10 mg) was mixed with epoxy resin (E44, 5 g), the curing agent (704, 5 g), and ethanol (5 g), and the organic coating was applied to the steel plate with a dipping machine. In order to investigate each component of HMTNs–BTA@ZnO-QDs on the performance of coatings, the coatings containing the HMNTs, HMNTs–BTA, or HMNTs@ZnO-QDs were also prepared by the same process.

2.4. pH-Responsive Test of ZnO-QDs. The ZnO-QD powder of 20.0 mg was mixed with 10 mL of pH buffer (pH of 7.0). The ZnO-QD aqueous solution with a concentration of 2.0 mg/mL was placed under UV light; 1.0 mol/L hydrochloric acid solution was then dropped to adjust the pH value of the solution to 2.0. After the dissolution of ZnO-QDs, 1.0 mol/L NaOH solution was added to the solution containing Zn^{2+} and to adjust the pH value to 12.0. At the same time, the optical photos before and after the disappearance of fluorescence and after the formation of white precipitation were taken. All optical photos were taken under the UV lamp at the wavelength of 365 nm. In order to avoid the uneven flow of the solution during adjustment of the pH, the whole process was carried out under the magnetic stirring of 100 r/min.

2.5. Experimental Test Methods. All electrochemical impedance spectroscopy (EIS) measurements were carried out on a VSP300 (Biologic) workstation over the frequency from 100 kHz to 0.01 Hz with an amplitude of 10 mV at room temperature. The traditional three-electrode system was used, where platinum sheet and Ag/AgCl were, respectively, used as the counter electrode and reference electrode. It is worthy to note that 5 min before EIS test, the open-circuit potential should not fluctuate more than 5 mV. All measurements are made in a self-made Faraday cage to avoid external interference.

2.6. Characterization. Scanning electron microscopy (SEM, Apreo s, America) was used to characterize the morphology of samples at an accelerating voltage of 5.0 kV. Coating samples with cross-sections were prepared with sandpaper and alumina polishing powder. Transmission electron microscopy (TEM, Tecnai G2 F20) was used to further observe the microstructure of materials. The N_2 gas adsorption–desorption isotherms of samples were measured on an ASAP-2020 analyzer. The BET model was used to calculate the specific surface area, and the non-local density function theory (NLDFT) method was used to calculate the pore volume and pore size distribution. An ultraviolet–visible spectrometer (L 5s) was used
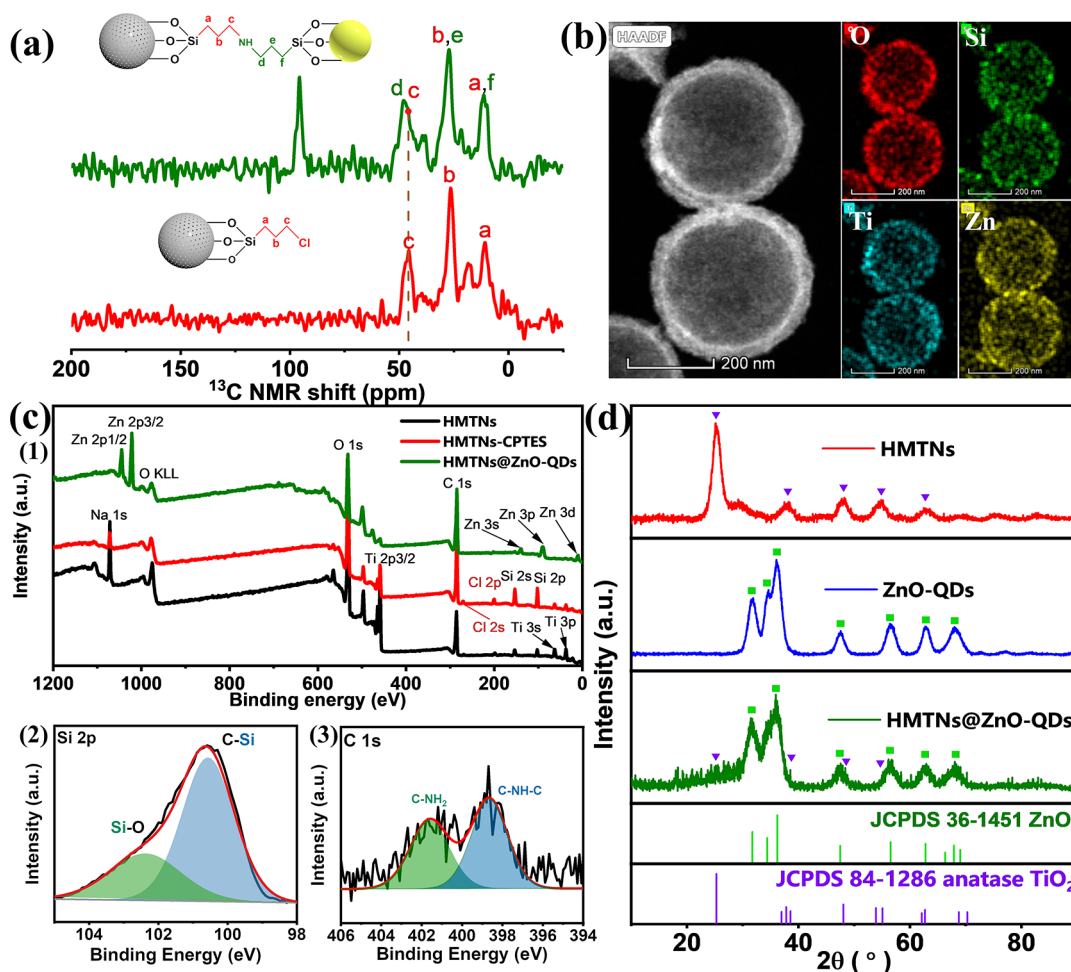
Figure 3. (a) ^{13}C SS-NMR spectra of HMTNs−CPTES and HMTNs@ZnO-QDs; (b) HAADF−TEM image of HMTNs@ZnO-QDs without loading BTA and the corresponding elemental mapping images; (c) XPS wide-scan spectra of functionalized HMTN materials, XPS high-resolution Si 2p core line spectra of HMTNs−CPTES, and high-resolution spectra of N 1s of HMTNs@ZnO-QDs; (d) XRD pattern of samples.

to detect the release of BTA caused by external pH changes. Usually, different pH values (2.0, 5.0, and 7.0) are adjusted with hydrochloric acid solution, and the solution is added to a cuvette. Then 10 mg/mL of the sample was put into the cone-shaped dialysis bag to soak it directly in the corresponding solution at 25 °C, and the ultraviolet−visible absorbance of the released BTA solution at 259 nm was recorded. A Fourier transform infrared (FT-IR) spectrometer (EQUINOX55) was used to record the FT-IR spectra of the solid sample. Thermogravimetric analysis (TGA) of samples was performed in a nitrogen atmosphere at temperatures of 30−800 °C with a heating rate of 10 °C/min using a TGA synchronous analyzer (SDT Q600). Crystalline structures were analyzed by X-ray diffraction (XRD) (D/MAX-2500X) with a Cu target (λ = 1.5406 Å) at an incident angle of 1 in the 2θ range from 10 to 90°. Solid-state nuclear magnetic resonance (^{13}C SS-NMR) was measured using a Bruker Avance 600 AV spectrometer, operating at a Larmor frequency of 100.6 MHz, and the magic angle spin rate was set to 10 kHz. X-ray photoelectron spectroscopy (XPS) analysis was performed on an AXIS-SUPRA spectrometer.

3. RESULTS AND DISCUSSION

3.1. Characterization of Nanocontainers. To store and release inhibitors uniformly and stably, nanocontainers with an excellent pore structure and size are requisite. In this study, the HMTNs were prepared by using SiO_2 as a template[27] and then used to store inhibitors. The preparation process of HMTNs is shown in Figure S1. The XRD pattern (Figure S2) shows the

characteristic peaks corresponding to the planes (101), (004), (200), (105), (211), and (204) of the highly crystallized anatase structure of TiO_2.[32] As shown in Figure 2a,b, HMTNs exhibit a good monodispersivity and an excellent hollow sphere with an outer diameter of about 260 ± 30 nm and a porous shell with a thickness of about 20 ± 5 nm. Therefore, HMTNs can supply a large hollow space to store a lot of BTA molecules. Moreover, the N_2 adsorption−desorption isotherms and the pore size distribution curves in Figure 2c show the typical type IV isotherm and H1 hysteresis loop, indicating a mesoporous structure of HMTNs. The pore size of the spherical shell is focused on 3.0 nm, which provides the important channels for the fill and release of corrosion inhibitors.

Once inhibitor molecules are filled into HMTNs, a sealing material is needed to avoid the leakage of inhibitors before corrosion. Because of the feature of small mesopores of HMTNs, the size of sealing materials must match the mesopores of HMTNs. In addition, the connection between the sealing material and nanocontainer must be considered. In this work, the amino-functional ZnO-QDs were prepared by the surface pretreatment method. With illumination from a fluorescent lamp and a UV lamp (256 nm), as shown in Figure 2d, the amino-functional ZnO-QDs exhibit an excellent dispersibility. It can be seen that the ZnO-QD solution
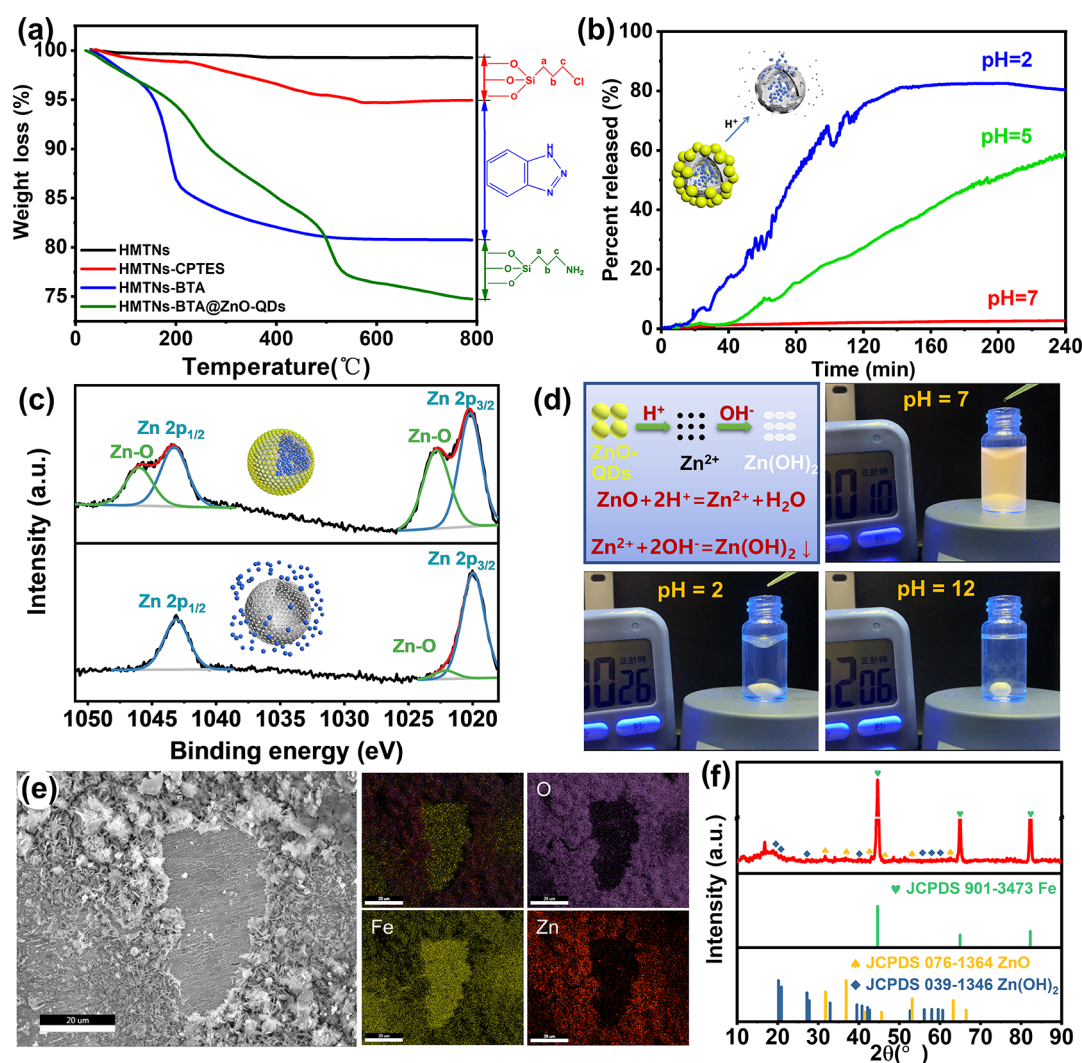
Figure 4. (a) TGA curves of samples; (b) acid-triggered release profiles of BTA from HMTNs−BTA@ZnO-QDs under different acidity values; (c) XPS high-resolution spectra of Zn 2p before and after the reaction with an acid solution of pH = 2; (d) optical microscopy photos of the decomposition time and white precipitate formation time of ZnO-QDs after continuous adjustment of pH = 2.0 (1 mol/L HCl) and pH = 12.0 (1 mol/L NaOH) under a UV lamp; (e) SEM image of the corrosion area on the surface of Q235 carbon steel immersed in 3.5 wt % NaCl solution containing ZnO-QDs (2 mg/mL) for 36 h and the corresponding elemental mapping images; (f) XRD pattern of the corrosion area.

displays a milky white color under the fluorescent lamp and the yellow color under the irradiation of UV light, indicating that the particle size ZnO-QDs should be more than 4 nm.[33] TEM images (Figure 2e) further illustrate that the diameter of the amino-functional ZnO-QDs is approximately 6.0 nm, which is big enough to seal the mesopores (3.0 nm) of HMTNs to avoid the spontaneous leakage of BTA.

In order to make a soft connection between the ZnO-QDs and HMTNs, their surface modifications were performed. The FT-IR spectrum (Figure 2f) confirms that ZnO-QDs have been connected with APTES. The new bond at 2933 and 2860 cm^{-1} in ZnO−APTES is assigned to C−H stretching vibrations.[12] The obvious absorption peaks around 1567 and 1102 cm^{-1} are attributed to the stretching vibration of the −NH$_2$ bond and Si−O−Si stretch vibration, respectively. Figure S3 shows the XPS spectra of ZnO-QDs and ZnO-QDs−APTES, which clearly indicate the new peaks of Si 2p and N 1s, illustrating that APTES has been grafted on the surface of ZnO-QDs. The aminated ZnO-QDs are a requisite to the HMTN sealing material since 3-aminopropyl can react with 3-chloropropyl groups of CPTES under certain

conditions.[34] Therefore, the surface of HMTNs was modified with CPTES in order to provide a soft connection point with ZnO−APTES for the efficient packaging of BTA.

Figure 3a presents ^{13}C SS-NMR spectra of the samples, in which HMTNs−CPTES exhibits a resonance signal of the propyl group at C_a (10.4 ppm), C_b (26.3 ppm), and C_c (45.4 ppm). The connection between ZnO-QDs and HMNTs can be produced through the reaction between the functional groups of APTES and CPTES. Compared with HMTNs−CPTES, the resonance signals in ^{13}C SS-NMR of HMTNs@ZnO-QDs corresponding to $C_{a,f}$ (11 ppm), $C_{b,e}$ (27.1 ppm), C_c (45.4 ppm), and C_d (47.8 ppm) demonstrate the complete combination of HMTNs with ZnO-QDs through the reaction of CPTES and APTES. More evidence can be found from the FT-IR spectra in Figure S4. The new bond at 2946 and 2883 cm^{-1} in HMTNs−CPTES can be attributed to the absorption peak of tensile vibration of the C−H bond. The stretching vibration absorption peak of C−Cl appears at 747 cm^{-1}. Compared with HMTNs−CPTES, HMTNs@ZnO-QDs has a new bimodal peak at 3300−3500 cm^{-1} due to the stretching vibration of N−H. Meanwhile, the flexural vibration absorption
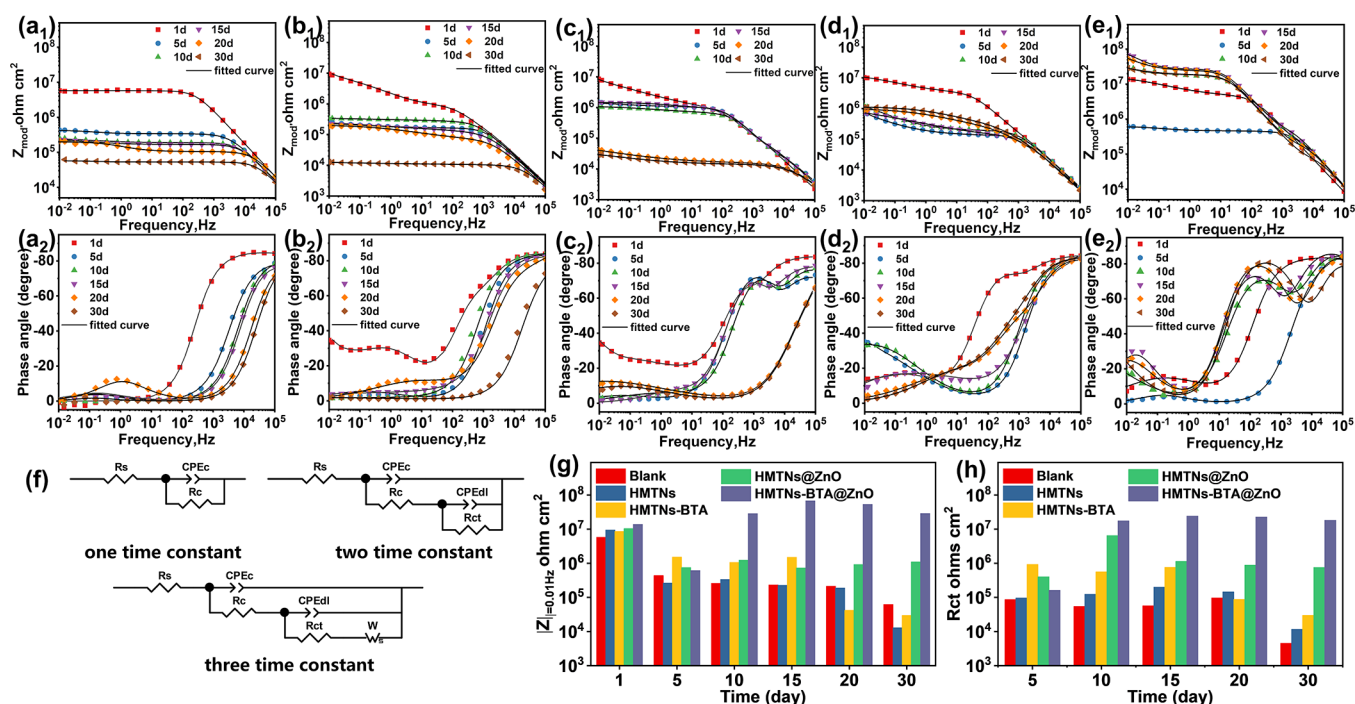
Figure 5. Bode plots and phase angle plots of the coatings immersed in 3.5 wt % NaCl with different times: epoxy coating (a_1, a_2), epoxy coating with HMTNs (b_1, b_2), epoxy coating with HMTNs−BTA (c_1, c_2), epoxy coating with HMTNs@ZnO-QDs (d_1, d_2), and epoxy coating with HMTNs−BTA@ZnO-QDs (e_1, e_2); electrical equivalent circuit used to fit the impedance data (f); evolution of $|Z|_{0.01\ Hz}$ (g) and R_{ct} (h) with immersion time. Here R_s is the solution resistance; CPEc and R_c are the capacitance and micropore resistance of the coating, respectively; and CPE$_{dl}$ and R_{ct} are the constant phase element and charge-transfer resistance of the double-layer capacitance, respectively. Warburg (W) is used to describe the phenomenon of tangential diffusion.[40] The appearance of W means that the metal begins to corrode.

peak corresponding to the primary amine N−H can be found at 1560 cm^{-1}, while the tensile vibration absorption peak of C−Cl disappears at 747 cm^{-1}, indicating that Cl has been replaced. TEM and energy-dispersive spectroscopy (EDS) were also used to observe the microstructure after the connection between the HMNTs and ZnO-QDs. As shown in Figure 3b, the morphology of HMTNs@ZnO-QDs maintains an excellent dispersibility and structural integrity. The EDS mapping images show the coexistence of O, Si, Ti, and Zn elements in HMTNs@ZnO-QDs. The results confirm that the functionalization and the connecting process do not alert the physical structure of nanocontainers.

Figure 3c shows the wide XPS scanning spectra of HMTNs, HMTNs−CPTES, and HMTNs@ZnO-QDs. The peaks of Cl 2s (269 eV) and Cl 2p (200 eV) can be observed in HMTNs−CPTES, indicating the successful functionalization process of HMTNs by CPTES. As shown in Figure 3d, after ZnO-QDs are grafted on the surface of the nanocontainer, the intensity of the diffraction peak of TiO$_2$ in HMTNs@ZnO-QDs is significantly reduced.[32,35] The corresponding variation trend can be also observed in the XPS wide spectrum compared with HMTNs−CPTES. The disappearance of the Ti 2p signal in HMTNs@ZnO-QDs and the appearance of Zn 2p (1022, 1044 eV) suggest that HMTNs are efficiently sealed by ZnO-QDs. In Figure 3c, the Si 2p spectrum of HMTNS−CPTES belongs to C−Si and Si−O groups at 100.5 and 102.4 eV, respectively. The N 1s spectrum of HMTNs@ZnO-QDs shows typical peaks at 398.7 and 401.6 eV, which are attributed to C−NH−C and C−NH$_2$, respectively.

3.2. Controllable Release of BTA from HMTNs. The loading amount of BTA in HMTNs−BTA@ZnO-QDs was first determined by TGA, and the results are shown in Figure

4a. The pristine HMTNs have only weight loss lower than 1.0% due to the absorbed water. After modification by CPTES, an obvious weight loss beginning at about 220 °C can be attributed to the decomposition of CPTES, which results in 5.0% weight loss. The weight loss of the HMTN filling with BTA begins at ambient temperature since BTA contains the physically absorbed water. A significant weight loss in the range of 150−520 °C can be attributed to the thermal decomposition of BTA and other organic substances. In addition to the absorbed water, CPETES, and BTA, a small portion of weight loss of HMTNs−BTA@ZnO-QDs can be attributed to the broken skeleton of the nanocontainer, when the temperature is over 520 °C. According to the TGA curves of samples, it can be calculated that the content of BTA filled in HMTNs−BTA@ZnO-QDs is approximately 14.2 wt %.

To investigate the controllable release behavior of BTA from nanocontainers, the release process was indicated by UV spectroscopy. During the test process, the nanocontainer was packed into a processed conical dialysis bag, which was then carefully placed in a quartz cuvette that was filled with a pH buffer solution. In order to obtain the reliable indicator of BTA, the standard BTA curve was also measured at a wavelength of 259 nm (Figure S5). Figure 4b shows the release content of BTA at pH from 7.0 to 2.0. It can be found that only 2.7 wt % BTA is slowly released from the HMTNs−BTA@ZnO-QDs within 4.0 h when the pH value of the buffer solution is 7.0, which should be ascribed to release of the BTA adsorbed on the surface of nanocontainers. It confirms that BTA can be well sealed in nanocontainers by ZnO-QDs when the electrolyte environment is neutral. When the pH value of the solution is adjusted to 5.0 and 2.0, respectively, it can be found that the corresponding release content of BTA reaches

59.6 and 82.5% after 4.0 h. The results indicate that the release efficiency of BTA has an obvious dependence on the acidity of the environment. The dependence derives from the response of ZnO-QDs on the acid solution. Once ZnO-QDs suffer the acid electrolyte to be dissolved, the mesoporous channels of nanocontainers are open to release BTA. From XPS analysis shown in Figure 4c, after the acid reaction, the peaks at 1022 and 1046 eV representing the ZnO−O chemical bonds disappear due to the dissolution of ZnO-QDs, which results in the elementary Zn to exist in the ionic state. The release efficiency of BTA depending on the decomposition rate of ZnO-QDs under acidic conditions is also demonstrated. ZnO-QD aqueous solution with a concentration of 2.0 mg/mL (pH of 7.0) was placed under UV light; 1.0 mol/L hydrochloric acid solution was then dropped to adjust the pH value of the solution to 2.0. As shown in Figure 4d, it can be found that the solution color of ZnO-QDs changes from yellow fluorescence to clear and transparent within 16.0 s due to the fact that ZnO-QDs can be rapidly decomposed once the environment becomes acidic. The results above well confirm that ZnO-QDs can play as a valve to control the release of BTA according to the environmental condition. Moreover, the effect of temperature on the decomposition rate of ZnO-QDs was tested. As shown in Figure S6, when the temperature increases from 30 to 80 °C, the decomposition time of ZnO-QDs shortens from 16 to 6 s. Correspondingly, the release rate of BTA will also increase to inhibit the corrosion of carbon steel.

To investigate the effects of Zn^{2+} resulting from the dissolution of ZnO-QDs on the corrosion process, 1.0 mol/L NaOH solution was dropped into the solution containing the ZnO-QDs after the response to the acidic signal of H^+ (pH of 2.0) to adjust the pH value to 12.0. As shown in Figure 4d, it can be seen that a large amount of white precipitates is formed in 2 min. The FT-IR of the white precipitate (Figure S7) displays the stretching vibration peak of OH^- at 3213 cm^{-1}. The OH^- of $Zn(OH)_2$ libration are observed at lower wavenumbers (1079, 1018, 933, and 848 cm^{-1}), indicating that the white precipitate is mainly composed of $Zn(OH)_2$.[36,37] The protective performance of the formed $Zn(OH)_2$ precipitation against the corrosion was evaluated by immersing the Q235 steel in 3.5 wt % NaCl solution containing 2 mg/mL (ZnO-QDs) for 36 h. From SEM images shown in Figure 4e, a large number of microparticles/nanoparticles result in a dense protective layer on the surface of carbon steel. SEM-elemental mapping image results show that they are mainly composed of Zn and O elements. From the XRD pattern shown in Figure 4f, the main composition of the protective layer is $Zn(OH)_2$ and ZnO. The above results show that the decomposed Zn^{2+} from ZnO-QDs can react with OH^- in the microcathode region of carbon steel corrosion to produce a protective layer composed of $Zn(OH)_2$ and ZnO. The influence of ZnO-QDs on the anticorrosion property of coating will be demonstrated in the following section.

3.3. Anticorrosion Property of the Coatings. EIS was conducted to evaluate the anticorrosion performances and the failure process of coatings. Figure 5a−e displays the time-dependent Bode modulus and phase angle plots of samples; the corresponding Nyquist curves are shown in Figure S8. Generally, a larger impedance modulus of $|Z|_{0.01\ Hz}$ means better anticorrosion performance. As shown in Figure 5g and h, after 1 day immersion, the $|Z|_{0.01\ Hz}$ value of coating with HMTNs−BTA@ZnO-QDs is $1.38 \times 10^7\ \Omega\ cm^2$, which is almost 2.4 times that of the pure epoxy coating. As the

immersion time increases to 5 days, $|Z|_{0.01\ Hz}$ decreases to about $6.12 \times 10^5\ \Omega\ cm^2$ for the coating with HMTNs−BTA@ZnO-QDs and $4.36 \times 10^5\ \Omega\ cm^2$ for the epoxy coating. Furthermore, after 5 days immersion, a new capacitance loop in the low-frequency area of Nyquist curves of Figure S8 indicates that the electrolyte has reached the interface of the coating and metal substrate to induce the occurrence of metal corrosion, which is mainly attributed to the resulting micropores during the curing process of epoxy coating. After 10 days of immersion, the $|Z|_{0.01\ Hz}$ value of epoxy coating still shows a downward trend, indicating that its protective property degrades. However, the $|Z|_{0.01\ Hz}$ value of coating with HMTNs−BTA@ZnO-QDs rebounds to $2.83 \times 10^7\ \Omega$ cm^2, which is even much higher than the $|Z|_{0.01\ Hz}$ of the coating immersed with 1 day. It can be attributed to the fact that the corrosion process causes the pH change of the microregion; once the environment becomes acidic, valves of ZnO-QDs are open to release BTA from HMTNs. The released BTA can produce a protective film on the surface of the metal substrate, which results in the higher corrosion resistance of the material.[37] It can also be noted in Figure 5d that a new peak at 5×10^3 Hz representing the time constant appears, which is a typical feature of BTA film formed on the surface of carbon steel.[38] As expected, even when the immersion time is up to 30 days, the $|Z|_{0.01\ Hz}$ value of HMTNs−BTA@ZnO-QDs coating still remains at 2.87×10^7 $\Omega\ cm^2$. The results well demonstrate the self-healing property and anticorrosion performance of the coating by the controllable release of BTA corrosion inhibitor.

Apart from $|Z|$ value, the resistance of charge transfer (R_{ct}) is an important indicator to evaluate the anticorrosion performance of coating, which can reflect the protectiveness of coating. To get the R_{ct} value of coatings, the equivalent circuit diagrams of Figure 5f were used to fit the Bode plots shown in Figure 5a−e; the results are shown in Figure 5h. It can be observed that the R_{ct} value of epoxy coating remains less than 8.57×10^4 $\Omega\ cm^2$ and has a trend of a decrease with immersion time since the protectiveness degrades with immersion time and the corrosion rate of the metal substrate increases. Although the epoxy coating with HMTNs−BTA@ZnO-QDs immersed for 5 days has almost the same R_{ct} value as the pure epoxy coating, it quickly increases by 200 times ($2.15 \times 10^7\ \Omega\ cm^2$) when the immersion time reaches 10 days and shows no change for 30 days. The results are highly consistent with the change of $|Z|_{0.01\ Hz}$ values of the coating and well prove the good self-healing performance of the coating containing HMTNs−BTA@ZnO-QDs.

To further understand the roles of BTA and ZnO-QDs on the performance of the coating with HMTNs−BTA@ZnO-QDs, EIS of the epoxy coating with HMTNs−BTA was compared with that of the other coating; it can be noted in Figure 5c2 that a new peak at 5×10^3 Hz representing the time constant appears for a middle immersion time (5−10 days).[39] It indicates that the BTA dispersed into the coating during the coating preparation is uncontrollable to release and to form the BTA film during the earlier stage of corrosion. When the epoxy coating with HMTNs−BTA was soaked to 20 days, the $|Z|_{0.01\ Hz}$ value sharply decreases, indicating that the BTA loses its protective effect. The results show that the uncontrolled release of BTA causes BTA to be consumed prematurely before corrosion occurs, so it is impossible to achieve efficient anticorrosion in the corrosion area.
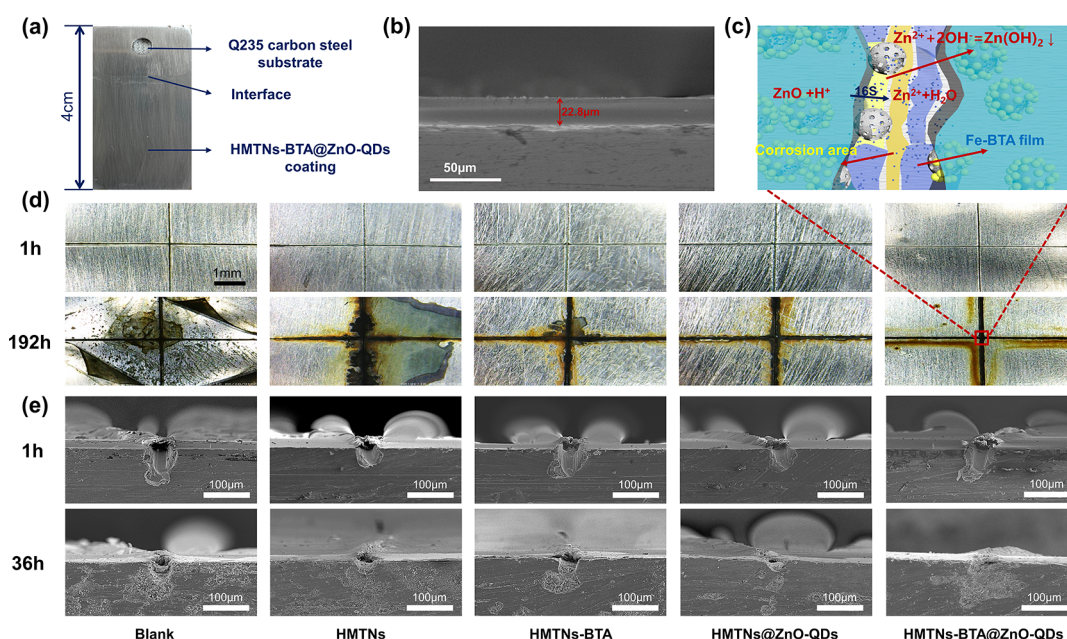
Figure 6. (a) Optical microscopy photograph of HMTNs−BTA@ZnO-QD coating deposited on carbon steel; (b) cross-sectional SEM images of HMTNs−BTA@ZnO-QDs coatings; (c) self-healing principle of the coating defect area; (d) optical microscopy photograph of the epoxy coating and the epoxy coatings with HMTNs, HMTNs−BTA, HMTNs@ZnO-QDs, or HMTNs−BTA@ZnO-QDs after 1 and 192 h of immersion; (e) cross-sectional SEM images of the epoxy coating and the epoxy coatings with HMTNs, HMTNs−BTA, HMTNs@ZnO-QDs, or HMTNs−BTA@ZnO-QDs after 1 and 36 h of immersion.

Interestingly, both the $|Z|_{0.01\ Hz}$ value and R_{ct} of the epoxy coating with HMTNs@ZnO-QDs are only inferior to those of the coating with HMTNs−BTA@ZnO-QDs for a long-period immersion test, suggesting that a protective film deriving from the conversion of ZnO-QDs is stably present for a long period. The protective film could be due to the fact that the responded dissolution of ZnO-QDs produces Zn^{2+} to react with OH^- of the cathode region to form the protective products of $Zn(OH)_2$, as confirmed by Figure 4e,f. EIS of the coating with HMNTs@ZnO-QDs (Figure S8d) also has the obvious diffusion phenomenon in the low-frequency region owing to the reaction of the decomposed Zn^{2+} with OH^- in the microcathode area. The results well demonstrate that the coating containing HMTNs@ZnO-QDs still exhibits a greatly enhanced anticorrosion performance for long-period tests even without addition of BTA.

The optical microscopy photograph of the coating with HMTNs−BTA@ZnO-QDs is shown in Figure 6a. The coating is colorless, transparent, and uniformly present on the carbon steel substrate. From the SEM image shown in Figure 6b, the coating is dense and compactly deposited on the substrate and has the thickness of 22.8 μm. In order to intuitively understand the anticorrosion performance and self-healing property of the coating with HMTNs−BTA@ZnO-QDs, all the coatings with the artificial scratches were immersed in 3.5 wt % NaCl solution and then the macroscopic morphology of the scratched areas was observed with an optical microscope. As shown in Figures 6d and S9, around the scratched area of the epoxy coatings and the epoxy coating with HMTNs, corrosion of the carbon steel matrix became more serious with immersion time. After immersion of 96 h, the coating had been peeled off and lost the protection on the metal. When the immersion time reached 192 h, the coating had completely lost its protectiveness and the substrate metal suffered a serious corrosion since the local degradation of the coating caused a

corrosion cell with a large cathode and a small anode. In contrast, the coatings with HMTNs−BTA and the coating with HMTNs@ZnO-QDs showed slight corrosion diffusion after immersion for 192 h. The coating with HMTNs−BTA was a little peeled off around the scratched area, but the coating with HMNTs@ZnO-QDs still showed a good adhesion with the metal matrix. When ZnO-QDs were used as the valves of HMTNs−BTA, the resultant coating maintains an excellent protectiveness on the metal matrix, and there are almost no breaks and peeling off in the coating. The results further indicate that the ZnO-QDs are vital to the controllable release of BTA and to produce the protective layers of $Zn(OH)_2$.

To investigate the contact between the coatings and the carbon steel matrix during immersion tests, the cross-sectional SEM images of samples were observed. As shown in Figure 6e, it can be found that if there are no ZnO-QDs, the addition of BTA does not enhance the adhesion between the coating and the matrix, suggesting that the uncontrollable release of BTA cannot improve the anticorrosion property of the coating. The introduction of ZnO-QDs can partially inhibit the gap formation between the coating and the carbon steel matrix due to the protective products from the responded dissolution of ZnO-QDs. In contrast, the coating with HMTNs−BTA@ZnO-QDs shows an excellent high adhesion, and the smallest gaps can be observed around the scratched area after immersion of 196 h. It further demonstrates the critical effects of ZnO-QDs on the excellent anticorrosion performance of the coating with HMNTs−BTA@ZnO-QDs. A response and self-healing principle of the coating is shown in Figure 6c. Once ZnO-QDs respond to the environmental signal of H^+ to be dissolved, the BTA loaded in HMNTs promptly releases to form the protective film of Fe−BTA on the surface of carbon steel to inhibit the corrosion of the metal matrix. On the other hand, the dissolved Zn^{2+} ions react with OH^- in the cathodic

area to produce the protective products of Zn(OH)₂, preventing the material from corrosion.

4. CONCLUSIONS

ZnO-QDs have been successfully used as the multifunctional valves to seal and controllably release the BTA inhibitor filling into the HMTNs. The results show that ZnO-QDs with a diameter of 6.0 nm can well match the pores of HMNTs to make the BTA sealed into the HMTNs with the pore size of 3.0 nm. On the other hand, ZnO-QDs can be efficiently dissolved to release BTA corrosion inhibitor once the pH value of the environment is lower than 7.0. Furthermore, the dissolved Zn^{2+} can react with OH^- in the cathodic region to produce the protective $Zn(OH)_2$ product. Therefore, when HMTNs−BTA@ZnO-QDs are used in epoxy coating, the coating exhibits a much higher corrosion resistance. After 30 days immersion in 3.5 wt % NaCl solution, the |Z| value at 0.01 Hz of the coating still maintains around $2.87 \times 10^7 \ \Omega \ cm^2$. Meanwhile, the sensitive response to the corrosion environment and the controllable release of BTA make the coating own an excellent self-healing property. The scratched tests demonstrate that the coating can well protect the metal matrix from corrosion owing to the controllable release of BTA corrosion inhibitor and the formation of the $Zn(OH)_2$ protective layer. After immersion in 3.5 wt % NaCl solution of 192 h, around the scratches of the coating, there is no delamination and corrosion of the metal is inhibited by the released BTAs and the protective layers of $Zn(OH)_2$.

■ ASSOCIATED CONTENT

Ⓢ Supporting Information

The Supporting Information is available free of charge at https://pubs.acs.org/doi/10.1021/acsami.2c16151.

> Preparation process of HMTN nanocontainers, XRD of HMTNs, fine spectra of Si 2p and N 1s in the modification process of zinc oxide quantum dots, FT-IR of the HMTNs@ZnO-QDs preparation process, UV−vis spectra of BTA, variation trend of decomposition time of ZnO-QDs with temperature, FT-IR of precipitates formed by Zn^{2+}, Nyquist curve of composite coating, optical microscopy photos of the scratched coating immersed in 3.5 wt % sodium chloride solution for different times, and effect of the amount of HMTNs−BTA@ZnO-QDs on the corrosion resistance of the coating (PDF)

■ AUTHOR INFORMATION

Corresponding Authors

Suning Li − *Key Laboratory of Energy Materials and Electrochemistry Liaoning Province, School of Chemical Engineering, University of Science and Technology Liaoning, Anshan 114051, China*; Email: suning7758@sina.com

Yiqing Chen − *State Key Laboratory of Metal Material for Marine Equipment and Application, Anshan 114009, China*; Email: chenyiqing@ansteel.com.cn

Zunfeng Liu − *State Key Laboratory of Medicinal Chemical Biology, College of Pharmacy and College of Chemistry, Tianjin 300071, China*; ⊙ orcid.org/0000-0002-7366-0275; Email: liuzunfeng@nankai.edu.cn

Baigang An − *Key Laboratory of Energy Materials and Electrochemistry Liaoning Province, School of Chemical Engineering, University of Science and Technology Liaoning,*
Anshan 114051, China; ⊙ orcid.org/0000-0001-6111-8166; Email: bgan@ustl.edu.cn

Authors

Zhaowen Tian − *Key Laboratory of Energy Materials and Electrochemistry Liaoning Province, School of Chemical Engineering, University of Science and Technology Liaoning, Anshan 114051, China*

Lixiang Li − *Key Laboratory of Energy Materials and Electrochemistry Liaoning Province, School of Chemical Engineering, University of Science and Technology Liaoning, Anshan 114051, China*

Zhizheng An − *Key Laboratory of Energy Materials and Electrochemistry Liaoning Province, School of Chemical Engineering, University of Science and Technology Liaoning, Anshan 114051, China*

Yanqiu Zhang − *Key Laboratory of Energy Materials and Electrochemistry Liaoning Province, School of Chemical Engineering, University of Science and Technology Liaoning, Anshan 114051, China*

Anqi Tong − *Key Laboratory of Energy Materials and Electrochemistry Liaoning Province, School of Chemical Engineering, University of Science and Technology Liaoning, Anshan 114051, China*

Han Zhang − *Key Laboratory of Energy Materials and Electrochemistry Liaoning Province, School of Chemical Engineering, University of Science and Technology Liaoning, Anshan 114051, China*; ⊙ orcid.org/0000-0001-6905-0952

Complete contact information is available at:
https://pubs.acs.org/10.1021/acsami.2c16151

Author Contributions

Conceptualization, S.L. and B.A.; methodology, Z.T.; validation, Z.A. and L.L.; formal analysis, Y.C. and H.Z.; data curation, A.T. and Y.Z.; writing—original draft preparation, Z.T.; writing—review and editing, S.L., Z.L., and B.A.

Notes

The authors declare no competing financial interest.

■ ACKNOWLEDGMENTS

■ REFERENCES

(1) Hou, B.; Li, X.; Ma, X.; Du, C.; Zhang, D.; Zheng, M.; Xu, W.; Lu, D.; Ma, F. The cost of corrosion in China. *npj Mater. Degrad.* **2017**, *1*, 1−10.

(2) Habibiyan, A.; Ramezanzadeh, B.; Mahdavian, M.; Bahlakeh, G.; Kasaeian, M. Rational assembly of mussel-inspired polydopamine (PDA)-Zn (II) complex nanospheres on graphene oxide framework tailored for robust self-healing anti-corrosion coatings application. *Chem. Eng. J.* **2020**, *391*, 123630.

(3) White, S. R.; Sottos, N. R.; Geubelle, P. H.; Moore, J. S.; Kessler, M. R.; Sriram, S.; Brown, E. N.; Viswanathan, S. Autonomic healing of polymer composites. *Nature* **2001**, *409*, 794−797.

(4) Shirehjini, F. T.; Danaee, I.; Eskandari, H.; Zarei, D. Effect of Nano Clay on Corrosion Protection of Zinc-rich Epoxy Coatings on Steel 37. *J. Mater. Sci. Technol.* **2016**, *32*, 1152−1160.

(5) Cui, G.; Zhang, C.; Wang, A.; Zhou, X.; Xing, X.; Liu, J.; Li, Z.; Chen, Q.; Lu, Q. Research progress on self-healing polymer/graphene anticorrosion coatings. *Prog. Org. Coat.* **2021**, *155*, 106231.

(6) Haddadi, S. A.; Ramazani S. A, A.; Mahdavian, M.; Taheri, P.; Mol, J. M. C.; Gonzalez-Garcia, Y. Self-healing epoxy nanocomposite coatings based on dual-encapsulation of nano-carbon hollow spheres with film-forming resin and curing agent. *Composites, Part B* **2019**, *175*, 107087.

(7) Leal, D. A.; Riegel-Vidotti, I. C.; Ferreira, M. G. S.; Marino, C. E. B. Smart coating based on double stimuli-responsive microcapsules containing linseed oil and benzotriazole for active corrosion protection. *Corros. Sci.* **2018**, *130*, 56−63.

(8) Izadi, M.; Shahrabi, T.; Ramezanzadeh, B. Active corrosion protection performance of an epoxy coating applied on the mild steel modified with an eco-friendly sol-gel film impregnated with green corrosion inhibitor loaded nanocontainers. *Appl. Surf. Sci.* **2018**, *440*, 491−505.

(9) Qian, B.; Zheng, Z.; Michailids, M.; Fleck, N.; Bilton, M.; Song, Y.; Li, G.; Shchukin, D. Mussel-inspired self-healing coatings based on polydopamine-coated nanocontainers for corrosion protection. *ACS Appl. Mater. Interfaces* **2019**, *11*, 10283−10291.

(10) Shchukin, D.; Möhwald, H. A coat of many functions. *Science* **2013**, *341*, 1458−1459.

(11) Guo, Y.; Wang, J.; Zhang, D.; Qi, T.; Li, G. L. pH-responsive self-healing anticorrosion coatings based on benzotriazole-containing zeolitic imidazole framework. *Colloids Surf., A* **2019**, *561*, 1−8.

(12) Wang, T.; Du, J.; Ye, S.; Tan, L.; Fu, J. Triple-stimuli-responsive smart nanocontainers enhanced self-healing anticorrosion coatings for protection of aluminum alloy. *ACS Appl. Mater. Interfaces* **2019**, *11*, 4425−4438.

(13) Yan, H.; Fan, X.; Cai, M.; Song, S.; Zhu, M. Amino-functionalized Ti3C2Tx loading ZIF-8 nanocontainer@ benzotriazole as multifunctional composite filler towards self-healing epoxy coating. *J. Colloid Interface Sci.* **2021**, *602*, 131−145.

(14) Shchukina, E.; Wang, H.; Shchukin, D. G. Nanocontainer-based self-healing coatings: current progress and future perspectives. *Chem. Commun.* **2019**, *55*, 3859−3867.

(15) Liu, C.; Zhao, H.; Hou, P.; Qian, B.; Wang, X.; Guo, C.; Wang, L. Efficient graphene/cyclodextrin-based nanocontainer: synthesis and host−guest inclusion for self-healing anticorrosion application. *ACS Appl. Mater. Interfaces* **2018**, *10*, 36229−36239.

(16) Hofmann, C.; Duerkop, A.; Baeumner, A. J. Nanocontainers for analytical applications. *Angew. Chem., Int. Ed.* **2019**, *58*, 12840−12860.

(17) Ding, J.; Zhao, H.; Shao, Z.; Yu, H. Bioinspired smart anticorrosive coatings with an emergency-response closing function. *ACS Appl. Mater. Interfaces* **2019**, *11*, 42646−42653.

(18) Jia, Y.; Qiu, T.; Guo, L.; Ye, J.; He, L.; Li, X. Preparation of pH responsive smart nanocontainer via inclusion of inhibitor in graphene/halloysite nanotubes and its application in intelligent anticorrosion protection. *Appl. Surf. Sci.* **2020**, *504*, 144496.

(19) Li, C.; Zhao, X. A.; Meng, M. A.; Zhang, T. A.; Sun, S. A.; Hu, S. Application of hollow mesoporous organosilica nanoparticles as pH and redox double stimuli-responsive nanocontainer in the controlled release of corrosion inhibitor molecules. *Prog. Org. Coat.* **2021**, *159*, 106437.

(20) Ding, C. D.; Xu, J. H.; Tong, L.; Gong, G.; Jiang, W.; Fu, J. Design and Fabrication of a Novel Stimulus-Feedback Anticorrosion Coating Featured by Rapid Self-healing Functionality for Protection of Magnesium Alloy. *ACS Appl. Mater. Interfaces* **2017**, *9*, 21034−21047.

(21) Zhu, Y.; Chen, M.; Wu, L. Synthesis of UV-Responsive Dual-Functional Microspheres for Highly Efficient Self-Healing Coatings. *Chem. Eng. J.* **2021**, *422*, 130034.

(22) Li, L. L.; Zheng, Z.; Möhwald, H.; Shchukin, D. G. Silica/polymer double-walled hybrid nanotubes: synthesis and application as stimuli-responsive nanocontainers in self-healing coatings. *ACS Nano* **2013**, *7*, 2470.

(23) Fu, J.; Chen, T.; Wang, M.; Yang, N.; Li, S.; Wang, Y.; Liu, X. Acid and alkaline dual stimuli-responsive mechanized hollow mesoporous silica nanoparticles as smart nanocontainers for intelligent anticorrosion coatings. *ACS Nano* **2013**, *7*, 11397−11408.

(24) Liu, X.; Gu, C.; Ma, Z.; Ma, X.; Hou, B. pH-Responsive containers based on modified hollow TiO2 for active and passive protection of carbon steel. *J. Electrochem. Soc.* **2018**, *165*, C145.

(25) Kcab, C.; Zyab, C.; Di, Y. Preparation of Ce-MOF@TEOS to enhance the anti-corrosion properties of epoxy coatings. *Prog. Org. Coat.* **2019**, *135*, 613−621.

(26) Xiong, H. M. ZnO nanoparticles applied to bioimaging and drug delivery. *Adv. Mater.* **2013**, *25*, 5329−5335.

(27) Muhammad, F.; Guo, M.; Qi, W.; Sun, F.; Wang, A.; Guo, Y.; Zhu, G. pH-Triggered Controlled Drug Release from Mesoporous Silica Nanoparticles via Intracelluar Dissolution of ZnO Nanolids. *J. Am. Chem. Soc.* **2011**, *133*, 8778−8781.

(28) Rostami, M.; Rasouli, S.; Ramezanzadeh, B.; Askari, A. Electrochemical investigation of the properties of Co doped ZnO nanoparticle as a corrosion inhibitive pigment for modifying corrosion resistance of the epoxy coating. *Corros. Sci.* **2014**, *88*, 387−399.

(29) Rassouli, L.; Naderi, R.; Mahdavain, M. The role of micro/nano zeolites doped with zinc cations in the active protection of epoxy ester coating. *Appl. Surf. Sci.* **2017**, *423*, 571−583.

(30) Roventi, G.; Bellezze, T.; Giuliani, G.; Conti, C. Corrosion resistance of galvanized steel reinforcements in carbonated concrete: Effect of wet−dry cycles in tap water and in chloride solution on the passivating layer. *Cem. Concr. Res.* **2014**, *65*, 76−84.

(31) Joo, J. B.; Zhang, Q.; Lee, I.; Dahl, M.; Zaera, F.; Yin, Y. Mesoporous anatase titania hollow nanostructures though silica-protected calcination. *Adv. Funct. Mater.* **2012**, *22*, 166−174.

(32) Shirke, B. S.; Korake, P. V.; Hankare, P. P.; Bamane, S. R.; Garadkar, K. M. Synthesis and characterization of pure anatase TiO2 nanoparticles. *J. Mater. Sci.: Mater. Electron.* **2011**, *22*, 821−824.

(33) Xu, X.; Xu, C.; Wang, X.; Lin, Y.; Dai, J.; Hu, J. Control mechanism behind broad fluorescence from violet to orange in ZnO quantum dots. *Crystengcomm* **2013**, *15*, 977−981.

(34) Dong, F.; Diao, S.; Ma, D.; Zhang, S.; Feng, S. Preparation and characterization of 3-chloropropyl polysiloxane-based heat-curable silicone rubber using polyamidoamine dendrimers as cross-linkers. *React. Funct. Polym.* **2015**, *96*, 14−20.

(35) Zhu, L.-P.; Liao, G.-H.; Huang, W.-Y.; Ma, L.-L.; Yang, Y.; Yu, Y.; Fu, S.-Y. Preparation, characterization and photocatalytic properties of ZnO-coated multi-walled carbon nanotubes. *Mater. Sci. Eng., B* **2009**, *163*, 194−198.

(36) Winiarski, J.; Tylus, W.; Winiarska, K.; Szczygieł, I.; Szczygieł, B. XPS and FT-IR characterization of selected synthetic corrosion products of zinc expected in neutral environment containing chloride ions. *J. Spectrosc.* **2018**, *2018*, 2079278.

(37) Lutz, H.; Jung, C.; Mörtel, R.; Jacobs, H.; Stahl, R. Hydrogen bonding in solid hydroxides with strongly polarising metal ions, β-Be(OH)$_2$ and ε-Zn(OH)$_2$. *Spectrochim. Acta, Part A* **1998**, *54*, 893−901.

(38) Hao, Y.; Zhao, Y.; Li, B.; Song, L.; Guo, Z. Self-healing effect of graphene@ PANI loaded with benzotriazole for carbon steel. *Corros. Sci.* **2020**, *163*, 108246.

(39) Calegari, F.; da Silva, B. C.; Tedim, J.; Ferreira, M. G.; Berton, M. A.; Marino, C. E. Benzotriazole encapsulation in spray-dried carboxymethylcellulose microspheres for active corrosion protection of carbon steel. *Prog. Org. Coat.* **2020**, *138*, 105329.

(40) Zheng, Z.; Schenderlein, M.; Huang, X.; Brownbill, N. J.; Blanc, F. d. r.; Shchukin, D. Influence of functionalization of nanocontainers on self-healing anticorrosive coatings. *ACS Appl. Mater. Interfaces* **2015**, *7*, 22756−22766.